DEVELOPMENT OF AN ADVANCED GAS TURBINE DRIVEN HIGH-SPEED CENTRIFUGAL PUMP FOR INJECTION SERVICES

by

Erio Benvenuti

Manager, Research and Development

Nuovo Pignone

Florence, Italy

and

Robert R. Ross

Vice President and Chief Engineer

United Centrifugal Pumps

San Jose, California

Erio Benvenuti is Manager of Turbomachine Fluid-dynamic Design and Analysis in the Research and Development Department of Nuovo Pignone. After receiving his degree in Mechanical Engineering, for over twenty years at Nuovo Pignone he has had part in a number of new achievements related to centrifugal and axial compressors, gas turbines and pumps, with contributions spanning from the setting up of design procedures through design and field performance assessment.

Mr. Benvenuti is a member of ASME, has authored many papers in turbomachine design and related theoretical and experimental fluid-dynamics. He has contributed as an instructor to education initiatives in Italy and abroad.

Robert R. Ross is Vice President and Chief Engineer of United Centrifugal Pumps. Prior to joining United, he was involved with centrifugal pump design with Weir Pumps, Ltd.

Mr. Ross received his Engineering degree in Scotland, and is listed in the Register of Chartered Engineers, is a registered professional engineer in the States of California and New Jersey, and is a member of the National Society of Professional Engineers. Mr. Ross is a Past President of the Hydraulic Institute.

He has authored several papers on centrifugal pumps, and is the co-author of the book, Centrifugal Pumps: Design and Application.

ABSTRACT

The high-speed centrifugal pump dealt with herein has been designed principally for applications in high-pressure injection for enhanced oil recovery. To assure the high output flexibility necessary for this service, the capability of varying the speed over a wide range was set as a main feature. For this purpose, a two-shaft gas turbine was chosen as a primary driver. Major design objectives were compactness, simplicity, and reliability. For achievement of the objectives, the direct coupling of the pump to the gas turbine as over 10,000 cpm, without gear, was set as a main goal. These primary objectives were associated with the request for modularity, ease of maintenance, high rotordynamic stabiity at all speeds, and good suction characteristics, to limit boosting requirements. A major support to this development was provided by high speed centrifugal compressor technology, from which design criteria and resources were applied to hydraulic and rotordynamic designs. A number of construction features, well proven on high pressure compressors, were implemented on this pump, through appropriate tailoring to the specific design objectives.

Testing at full power and speed of a complete high speed pump and gas turbine set demonstrated satisfactory agreement of the actual performance with the related design objectives.

INTRODUCTION

High-pressure injection for enhanced oil recovery has been the subject of growing interest from the oil industry in the last few years. For this service, reliability and availability of equipment are major requirements to assure pressure maintenance in reservoirs and to guarantee continuity to the strong increases in oil production achieved. Reliability, ease of transport and erection on site, and quick and simple maintenance are important features in view of the remoteness and adversity of environmental conditions typical of many oil fields. The need for equipment of this kind led the companies involved to decide to complete the top segment of their pump lines with a high speed unit to be applied principally, although not exclusively, to injection services.

A major design objective was that of achieving the widest possible operating range, to promptly respond to the changes in capacity and head which are often required in exploitation of oil wells. A variable speed, gas turbine driven assembly resulted as the most appropriate, especially for high power applications. Direct pump and gas turbine coupling without the need for an intermediate gear was set as a primary design objective to assure maximum simplicity, compactness and reliability. This feature called for a pump capable of operating at over 10,000 cpm with powers up to 6,000 hp and speeds variable in the 50 percent to 100 percent range, to match the characteristics of the two-shaft gas turbine selected.

The following more specific objects were set to match and complete the primary objectives:

- Full integration of the auxiliaries and mechanical components of the pump and gas turbine.

• Modularity, to meet the requirements of different applications with limited changes to the hardware.
• Easy and quick maintenance.
• Stable rotordynamic behavior over the full speed-range potential of a two-shaft gas turbine.
• Good efficiencies over a wide range of capacities and heads to utilize the turbine power range with a limited number of pump models.
• Moderate cavitation-free $NPSH_R$, to limit suction boosting requirements.

To cut the development time and to minimize risks, extensive use was made of in-house design resources and know-how related to industrial, highspeed centrifugal compressors. Therefore, the pump design could benefit from a wealth of knowledge in centrifugal stage fluid-dynamics [1, 2] and high speed rotordynamics [3]. In the next sections, an overview on the pump development steps will be given, including the layout of the machine architecture, the detailed hydraulic and mechanical design, the final performance assessment through full power and speed testing of a complete pump and gas turbine set.

PUMP ARCHITECTURE AND FUNCTIONAL FEATURES

The requirements associated with the objectives of compactness, structural simplicity, simplified installation and maintenance, and safe rotordynamic behavior guided the layout of most of the pump architecture (Figure 1). In turn, this basic layout set a number of constraints around which the successive hydraulic design was developed and optimized. A description of the most relevant pump features is presented briefly here as an introduction to some key aspects of the hydraulic and mechanical designs.

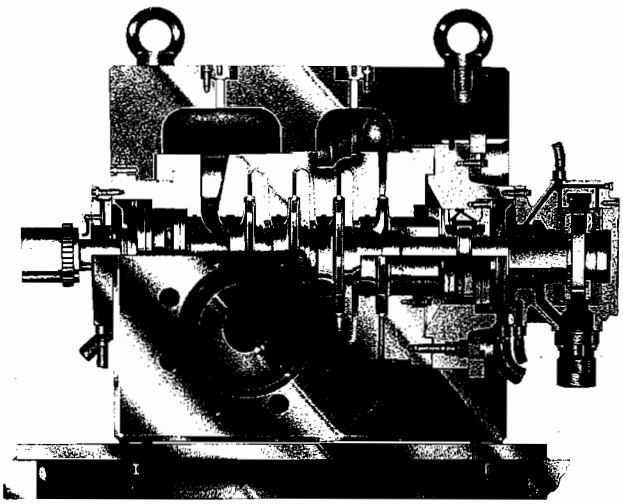

Figure 1. High-Speed Four-Stage Centrifugal Pump.

According to the philosophy of utilizing appropriate centrifugal-compressor-design know-how, reference was made to features successfully implemented on units which had been developed principally for very high pressure natural gas reinjection (Figure 2). The most significant compressor features included in the design of this high speed pump are:

• Barrel-type outer casing to allow for operating discharge pressures up to 400 bars, with a single end cover locked by a shear-ring fixture.
• In-line impeller layout with radial diffusers, cross-over bends and return channels (Figure 3). This configuration favors the modularity of stage components and requires shorter rotor lengths with respect to a back-to-back arrangement.

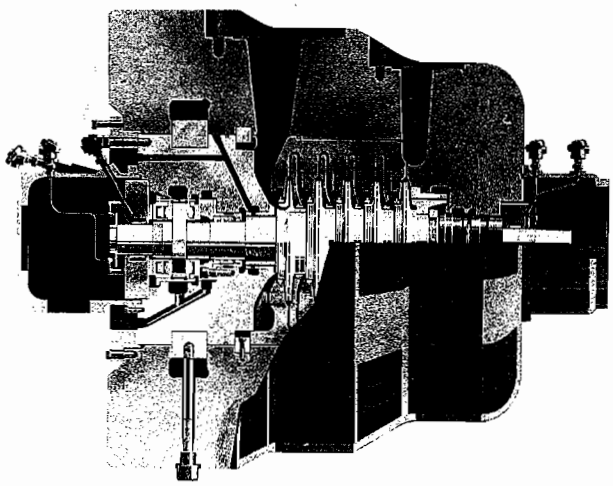

Figure 2. Very High Pressure Centrifugal Compressor.

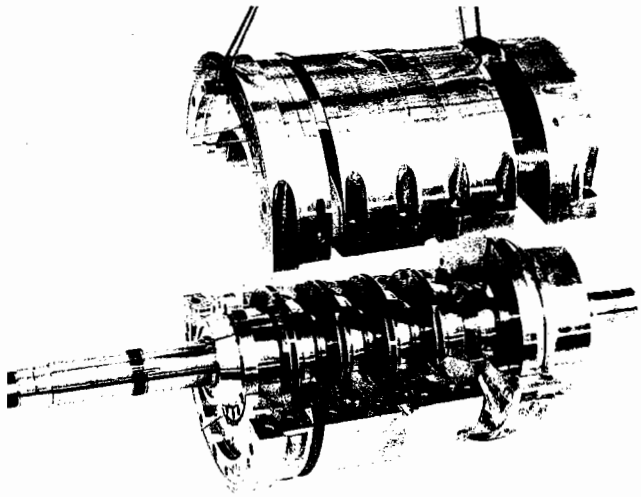

Figure 3. Split Diffuser Diaphragms Installed in Split Inner Case.

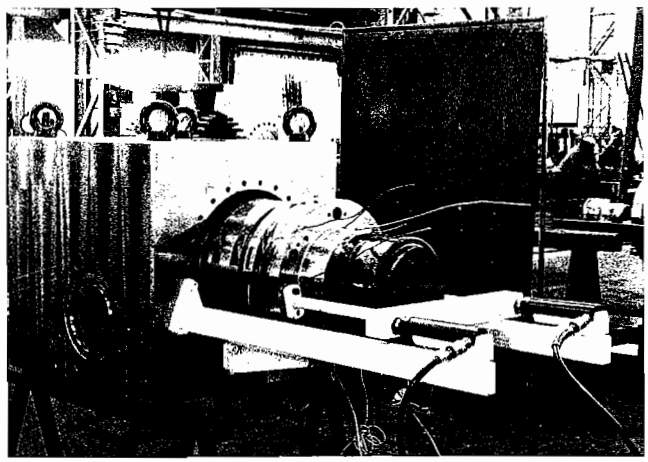

Figure 4. Extracting of the Inner Diaphragm and Rotor Cartridge Assembly.

• Horizontally-split interstage diffuser diaphragms enclosed by a horizontally-split inner casing. They form a single cartridge that can be extracted from the outer barrel without disconnecting the main piping (Figure 4).

• Small stage pitch and relatively large shaft-to-impeller diameter ratio, to make the rotor as short and rigid as possible. Besides the advantages in reliability provided by a stiff rotor in normal operation, this feature makes dry running at full speed possible with no risks.

A feature peculiar to this pump design is the square outer casing cross-section, that eliminates the need for welded support feet and welded suction and discharge flanges (Figure 4). Due to the complete absence of weldings, the casing can be manufactured from a single, compact stainless steel forging.

To achieve long, reliable operation in severe services like sea water pumping, all materials have been selected to resist corrosion and erosion. Techniques for applying and machining hard surface coatings on duplex stainless steel have been appropriately selected and thoroughly checked for the parts subject to wear.

The pump skid is designed to be directly bolted to one end of the gas turbine baseplate (Figure 5). This feature, associated with both the absence of a gear and the common turbine and pump lube oil system, results in a self-contained asembly which is easy to transport and install. It is well suited, for example, to off-shore applications.

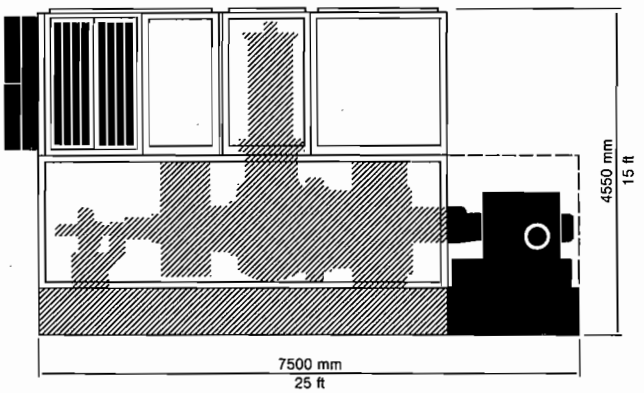

Figure 5. High-Speed Pump and Industrial Two-Shaft Gas Turbine Coupled to Form an Integral Module.

The design of the suction nozzle is very important to achieve reasonable cavitation-free net positive suction head required ($NPSH_R$). Implementing a pump nozzle with continuously variable flow areas inside the barrel was not practical. Therefore, the intake was made with a large annular duct cut in the barrel wall. This duct distributes the flow circumferentially to a radial accelerating channel provided with six support and flow straightening struts. This type of intake, with very low velocities in the annular duct, is widely used on many turbomachines other than pumps. When properly sized, it produces very low flow distortions and pressure drops at the impeller inlet. Instead, a variable-area volute is provided at the discharge by a cast inset placed inside the exit annular duct.

Lastly, the objective of utilizing the full range of the gas turbine power can be achieved with few changes to the pump hardware, as shown in the performance chart in Figure 6. All the heads and capacities within the range, which is bounded by the turbine power limit lines, can be reached with only four different specific speed pump models. The extra ranges made available by the same models can, in turn, be effectively exploited by using other types of drivers.

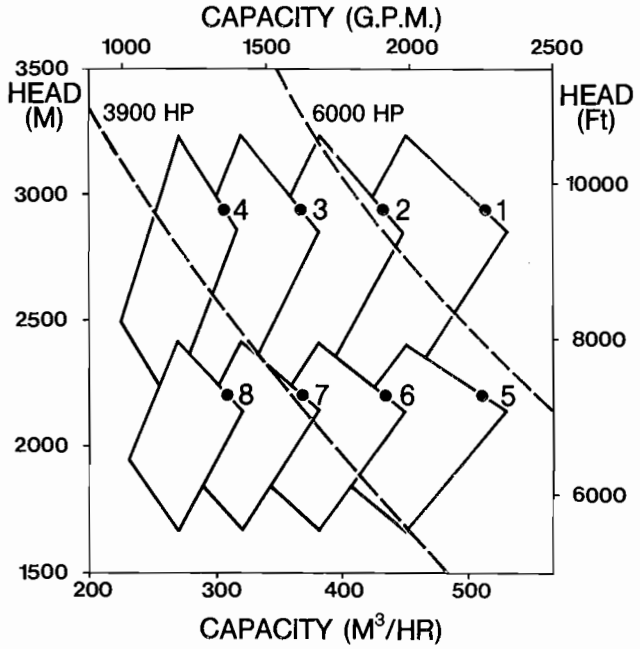

Figure 6. High-Speed Pump Performance Chart.

STAGE HYDRAULIC DESIGN

Parametric Design Optimization

The hydraulic design was developed according to a performance specification set as representative of a high-pressure water injection service, requiring full gas turbine power, i.e., 6,000 hp for average site conditions.

The overall pump head resulted in 3,000 meters (m) (9840 ft) for a design water capacity of 400 m^3/hr (1760 gpm). The direct coupling to the gas turbine called for a shaft speed of 10,290 cpm.

A parametric study was performed to evaluate the optimum number of stages. Constraints for the possible choice were the in-line stage layout with small axial pitch, short radial diffusers to limit the outer casing size, identical impeller on all stages, shaft diameters as large as possible. Component hydraulic efficiencies were estimated by means of correlations allowing fluid-dynamic, leakage, and impeller-disk-friction losses to be evaluated individually.

In Figure 7, predicted stage hydraulic efficiencies are plotted as a function of stage number and corresponding specific speeds. The four-stage efficiency was set as the reference. Only marginal benefits in efficiency are possible with more than four stages. Moreover, additional stages could impair the rotordynamic behavior, because of the need for long and flexible rotors. The four-stage configuration with 250 mm (9.8 in) impelllers was therefore selected as the best trade-off between the efficiency target and the objective of achieving a compact asembly with a rigid rotor. The successive selection of the impeller design parameters was directed towards keeping flow recirculation as far as possible from the design capacity, as a contribution to the reliability objective. In high-speed pumps with elevated fluid energies, in fact, suction and discharge impeller recirculation can produce blade erosion, axial movements of the shaft and damage to the thrust bearing [4, 5[, thus impairing reliability. The goal of delaying discharge recirculation led to choosing a relatively large blade number (seven) and an exit flow coefficient C_{m2}/U_2(C_{m2} = impeller exit meridional velocity, U_2 = tip speed) in excess of 0.10. This is a fairly high

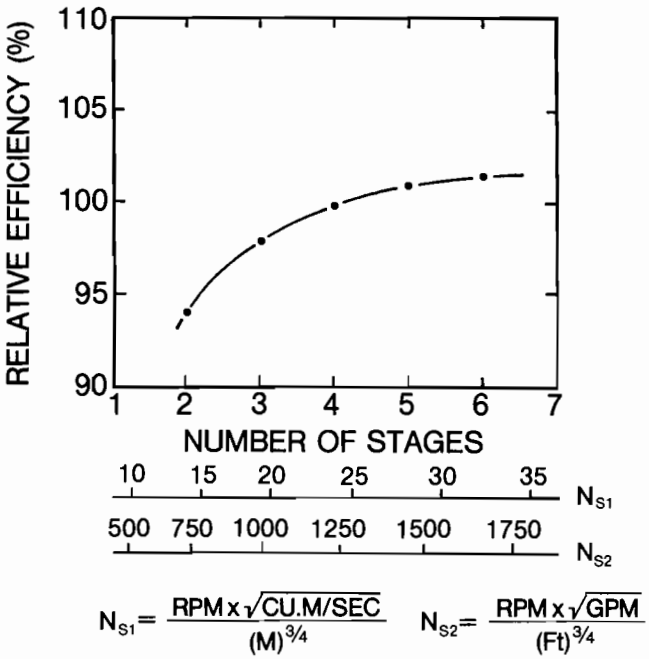

Figure 7. Predicted Efficiency Trends vs. Stage Number.

design value for a pump impeller with a 22 degree exit blade angle.

A similar goal for suction recirculation was pursued by keeping the impeller inlet eye area below values recommended for a very low cavitation-free $NPSH_R$ [5]. This resulted in somewhat high blade-inlet angles (over 20 degrees at shroud); they, in turn, reduced the inlet blockage due to the blade number, thus limiting the drawbacks of a narrow inlet eye area on $NPSH_R$.

The radial space left available by the mechanical sizing of the inner and outer casing imposed a limit of 1.3 for the diffuser-to-impeller exit radius ratio. This value is below the limit indicated by experience as a minimum for user of vaneless diffusers without appreciable efficiency penalties. Therefore, vaned diffusers were provided on all the stages to assure sufficient energy recovery in the short radial space available downstream from the impeller.

Impeller Design

The impeller blade design was performed using a computer-assisted, interactive procedure routinely used for compressors and for specific design updates on impellers of current production pumps. The procedure consists of several steps, the most important being the detailed analysis of the flow both upstream of the impeller and inside the blade-to-blade space. The first of these analyses is used to optimize wall curvatures for minimum flow accelerations on the flowpath upstream of the impeller, while the second one serves to optimize the blade shape.

A complete impeller blade design consists of the following main steps:

• Optimization of the blade entrance region for a given inlet eye area. This is achieved by minimizing the relative inlet velocity at the blade leading edge and the successive flow acceleration and pressure drop on the back (or suction side) of the blade. In compressor design, this step is very important when dealing with impellers operating at high inlet Mach numbers. In these cases, uncontrolled flow accelerations on the blade suction side can easily lead to local supersonic velocities and high shock wave losses, associated with flow choking at the throat. In high-speed-pump impellers, especially with a relatively small eye area, a good control of flow inlet velocity and acceleration over the blade is effective in reducing both the static pressure drop and the related cavitation-free $NPSH_R$.

• Control of the work transfer from the blade to the fluid. The work passes from the impeller to the fluid via the differential pressure arising between the front (or pressure) and the suction side of each blade. This results in a difference between the relative flow velocities Ws and Wp on the two sides respectively. The local intensity of work transfer is expressed by the "Loading Factor:"

$$LF = \frac{Ws - Wp}{Wm}$$

where Wm = mean blade-to-blade velocity

Its distribution over the impeller blade length is very important for controlling flow deceleration over the blade and preventing premature separation.

• Detailed specification of the three-dimensional blade geometry to be used for manufacture, either by casting or by five-axis milling from solid forgings. Although case impellers were selected for the initial high-speed pump units, the milling capability is available for flexibility in providing individually customized designs.

The front view of the blade shape along the shroud is shown in Figure 8. The tapered, initial blade portion is a result of iterations aimed at minimizing flow acceleration after the leading edge. The results of this effort are visible in Figure 9, showing relative velocity distributions over the blade surfaces along the shroud. The suction-side flow acceleration from the leading edge up to the throat is below ten percent of the relative inlet velocity. This is a good result when considering the relatively high blade number and the pronounced shroud wall curvature needed to limit the axial pitch. The associated static pressure drop between the leading edge and the throat is therefore small, thus partly off-setting the undersizing of the inlet eye area.

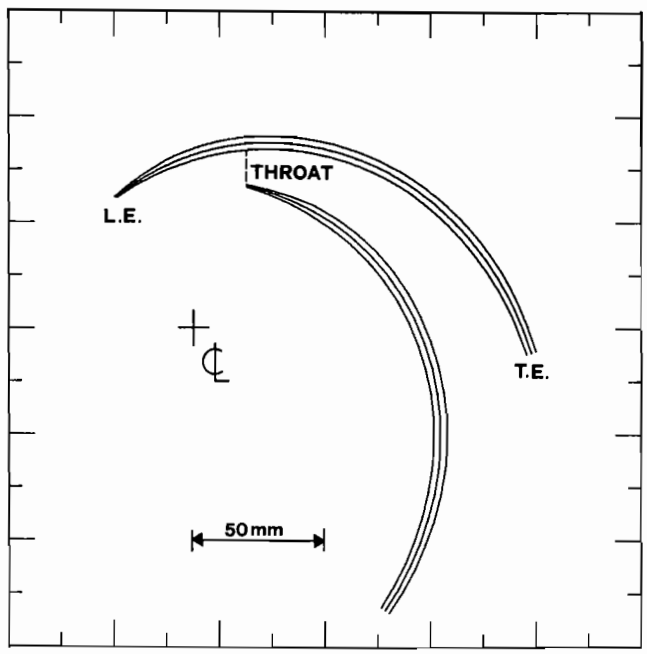

Figure 8. Front View of Impeller Blades at Shroud.

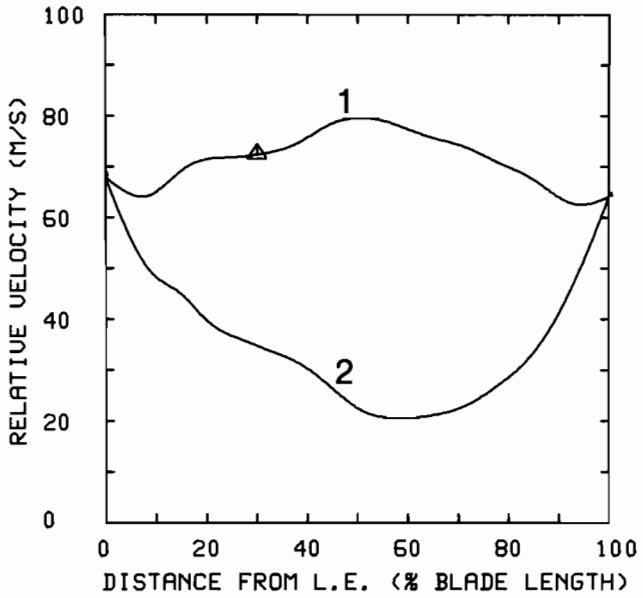

Figure 9. Predicted Relative Velocity Distributions at Shroud.

The loading factor diagram (Figure 10) drawn from the Figure 9 velocity distributions, shows that maximum loading is attained on the central blade portion. The low initial loading is a result of the blade-shape optimization, aimed mostly at controlling NPSH. The limited loading at exit is a result of the blade number and shape, and of the discharge flow coefficient C_{m2}/U_2, that was made higher than values typical of low speed pumps.

A maximum loading location closer to the blade exit would result from a smaller blade number and a lower exit flow coefficient. It would lead to greater flow deceleration on the pressure side, thus bringing the conditions for flow separation closer to the design point. When reducing the pump capacity, the blade exit loading increases and the pressure-side minimum velocity drops further. Flow separation with exit recirculation can, therefore, be initiated at relatively high capacities, if the blade exit loading at design capacity is too high.

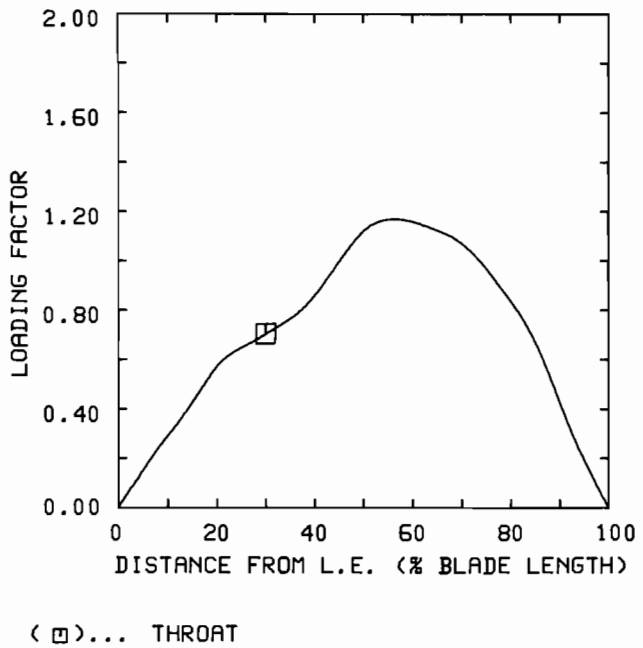

Figure 10. Impeller Blade Loading Factors at Shroud.

Although applying blade loading criteria is a fairly common practice in compressor design, published literature gives little evidence of a similar situation in the pump world. Based on the authors' experience in compressor development, where similar criteria led to significant achievements in impeller-flow stability, such a practice was implemented with confidence in the design of this pump. This choice was supported also by the limited literature found on this subject in relation to pumps [6].

The constructional shape of the impeller blades can be seen in Figure 11, showing the metal pattern used for producing the ceramic cores, and made by five-axis numerically controlled (N.C.) milling, with geometric data automatically generated by the computer design package.

Figure 11. Impeller Blade Ceramic Core Metal Pattern.

Diffuser Design

To avoid high losses in the 180 degrees cross-over bend due to the wakes from the short diffuser vanes, these were made continuous with the return channel vanes. For this design, a channel type diffuser with wedge vanes was chosen. The drawback of large wakes behind the thick trailing edges was eliminated by the continuity with the return vanes. The actual diffuser-return channel assembly can be seen in Figure 12. In this configuration, little diffusion occurs on the front side and none along the 180 degrees cross-over. Most diffusion is, therefore, accomplished in the return channel, not affected by incidence on changing capacities. These features contributed considerably to the wide stage operating range demonstrated in the fluid-dynamic tests following the design.

MECHANICAL DESIGN

Component Stress Analysis

All major components were stress-analyzed via detailed three-dimensional finite-element models. The analyses included the impeller, outer and inner casing, and the interstage diaphragms. The impelller stress analysis was principally aimed at carefully evaluating its interference with the shaft at operating speed. This check was needed to assure the appropriate contact pressure for

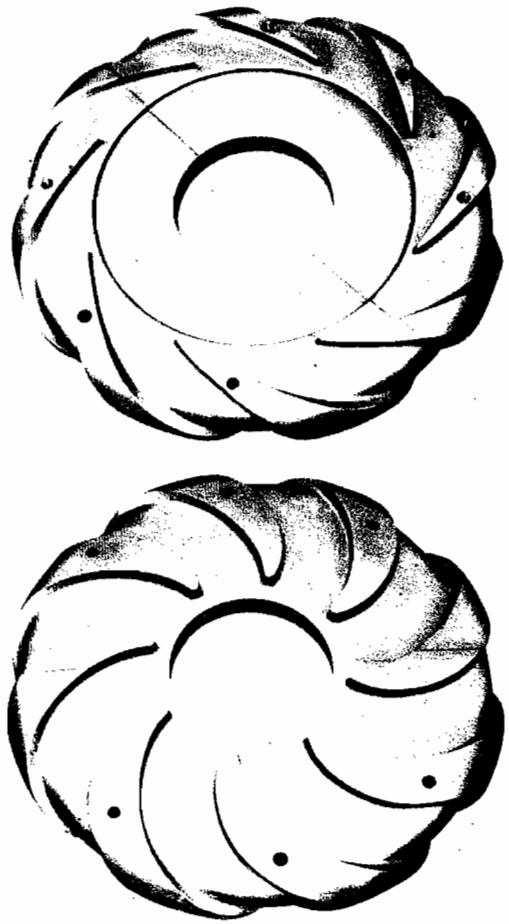

Figure 12. Integral Vaned Diffuser and Return Channel Assembly. (Upper view: front side, lower view: return channel).

transmitting torque without tangential keys. Avoiding the use of impeller keys permitted smaller hub geometry. For maximum accuracy, fluid pressures calculated in the hydraulic analysis were included in the finite-element model, in addition to centrifugal forces and shrink pressure.

The full three-dimensional finite-element model of the impeller is shown in Figure 13, and the calculated constrant stress lines appear in Figure 14. The maximum ideal stress levels observable do not exceed 5 kg/mm^2 (7.1 × 10^{3}psi).

Rotordynamic Analysis

From the pump design outset, rotordynamics considerations led to important choices in the overall architecture. These

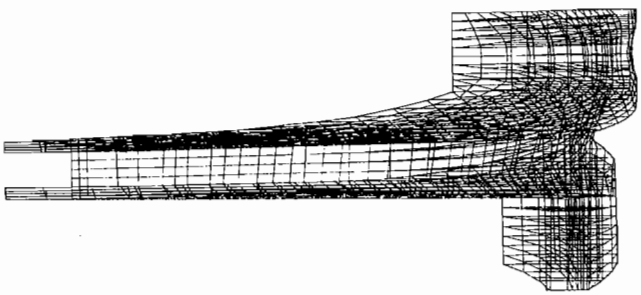

Figure 13. Impeller Finite-Element Model for Stress Analysis.

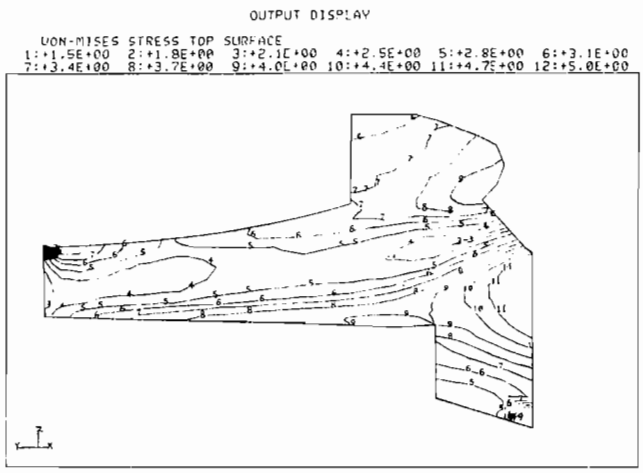

Figure 14. Impeller Ideal Stress Distribution.

considerations yielded the inline impeller layout with short stage pitch and suitably large shaft diameters, and the use of high damping tilting-pad radial bearings.

Among several types of rotordynamic predictions which were made, one deserving much attention was the rotor damped natural frequency and logaritmic decrement analysis [7].

The tilting pad bearings utilized on this pump are of a standard type developed for high speed compressors. The stiffness and damping coefficients needed for the rotordynamic analysis were therefore available and well validated. In normal wet operation, wear rings and, chiefly, the balance-piston seal can act like additional bearings. The related film stiffness and damping coefficients must, therefore, be accounted for in the rotordynamic analyses. For their evaluation, a simplified approach like that of Lomakin [8] was deemed sufficiently accurate in this case. Maximum shaft eccentricities do not, in fact, exceed 50 percent of the radial clearances, thus making the use of a more refined analysis unnecessary.

Rotor damped vibration frequencies and logarithmic decrements for dry and wet operation are summarized on the Campbell diagrams of Figures 15 and 16, respectively. In dry running conditions (Figure 15), the intersections of the one per

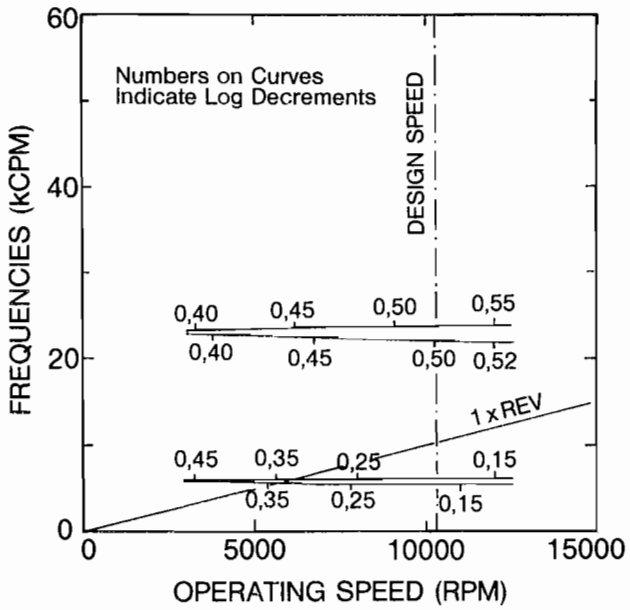

Figure 15. Campbell Diagram of Rotor for Dry Running.

revolution frequency line with rotor mode lines occur at around 6000 cpm. This can be considered as the conventional first rotor critical speed with finite stiffness bearings. A positive log decrement around 0.4 indicates that sufficient damping is available for safely crossing this critical speed in dry running. For normal wet operation, in the presence of the wear ring and balancing drum seal liquid films, the Figure 16 Campbell diagram shows no resonances. Very high log decrements for all rotor modes are a further guarantee of stable operation at all speeds.

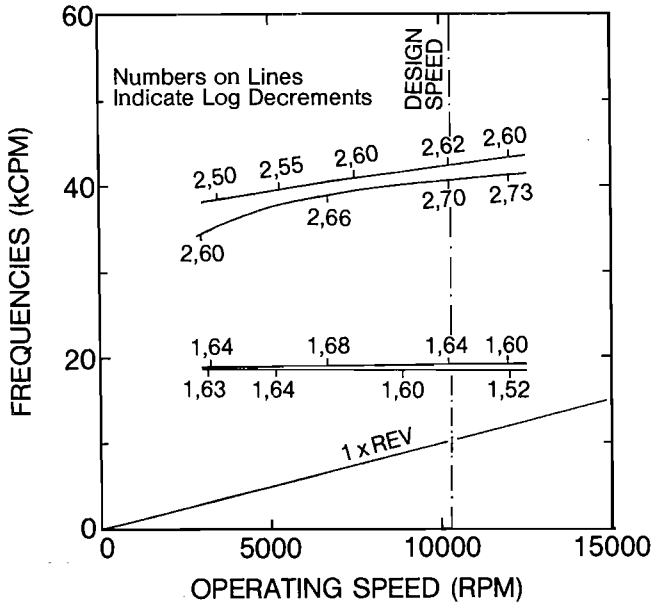

Figure 16. Campbell Diagram of Rotor for Wet Running.

COMPONENT TESTING AND TUNING

Factory testing of complete, high power turbomachines is very expensive for both energy consumption and the complexity of organization and services required. Costs increase rapidly if modifications to components are needed at this stage. Therefore, it is advisable to perform extensive testing and tuning of important components during the development of major projects. This practice can avoid delays, costs, and risks associated with modifications needed during the functional tests of completely assembled machines.

Low-Speed Stage Hydraulic Testing

Stage fluid-dynamics is very important in determining performance and is difficult to significantly change on assembled machines during testing. Therefore, a single pump stage was extensively tested hydrodynamically on a new facility (Figure 17), set up on the basis of multi-year experience on similar rigs utilized for centrifugal compressors [1, 2].

The pump stage rig is a low speed (2,980 cpm) test facility; the improvements in evaluating stage performance on a full speed rig were evaluated as too marginal to justify the far larger associated costs.

Many pressure measurements are located along the flowpath. They included fixed total-pressure-probe rakes at the stage inlet and exit. Traversable directional probes are present at the impeller discharge to measure the diffuser inlet flow conditions. Efficiency is evaluated through both the power absorbed by the electric motor and measured shaft torque. A vacuum tank on the suction line is used for cavitation tests.

The initial stage tests were utilized principally to check impeller and diffuser matching. A narrower than required diffuser

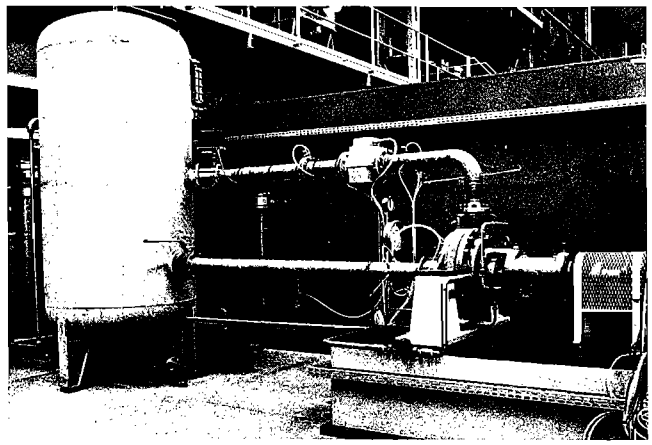

Figure 17. Low Speed Pump Stage Test Facility.

throat resulted, with a two to three precent penalty in the best stage efficiency. The throat was, therefore, opened 15 percent, through a slight modification to the vane leading edge portion.

The low-speed stage performance curves after diffuser rematching (Figure 18) show the best efficiency point close to 120 m^3/hr, corresponding to the 400 m^3/hr full speed design capacity. A maximum overall stage hydraulic efficiency around 78 percent was beyond expectations for this design in the medium to low specific speed range. The good diffuser energy recovery and, principally, its correct matching to the impeller, played a major role in achieving this higher than average performance.

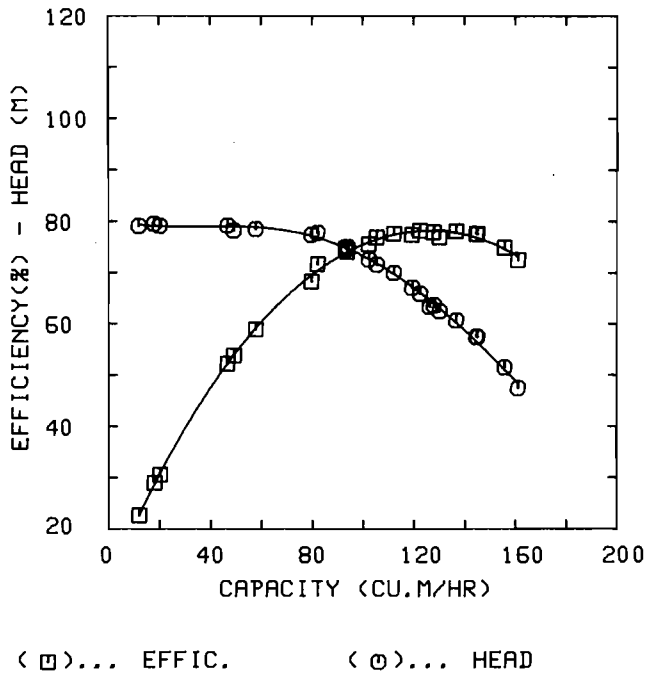

Figure 18. Low Speed Test Performance.

The diffuser characteristics in terms of inlet kinetic head recovery and of total pressure loss coefficients are shown in Figure 19, respectively. The loss coefficient remains flat in a large range from 40 percent to 125 percent of the best efficiency point (BEP) capacity, and doubles only below 20 percent of BEP capacity. This flat diffuser loss curve, associated with the impeller blade exit backslope, contributes to the achievement of the continuously rising head-capacity line at decreasing flows in Figure 18.

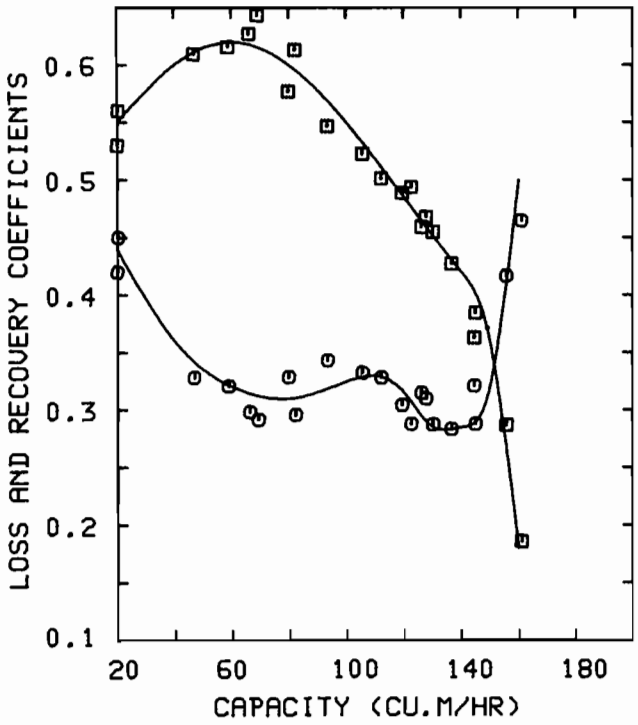

(□)... RECOVERY (○)... LOSS

Figure 19. Diffuser Experimental Performance Coefficients.

Inlet flow recirculation was detected by observing when the total pressures measured upstream of the impeller eye dropped below the corresponding wall static pressures, and appeared between 25 percent and 30 percent of the BEP capacity. Based on the authors' experience, this is a low value for a pump in this specific speed and suction specific speed range.

Results of cavitation tests at 2,980 cpm are summarized in Figure 20, where heads at five different flows are plotted versus suction pressures. $NPSH_R$ values at three percent head loss were lower than predicted and compared favorably with cavitation-free $NPSH_R$ evaluated at BEP (Figure 21). For the calculations, cavitation free $NPSH_R$ is expressed as:

$$NPSH_R = K_1 C_{m1}^2/2g + K_2 W_1^2/2g$$

where

K_1 = friction and acceleration loss coefficient
K_2 = blade entry loss coefficient
C_{m1} = average meridional velocity at blade inlet (m/sec)
g = gravitational acceleration (m/sec^2)
W_1 = relative velocity of flow at blade inlet

As cavitation is most likely to occur in the region where relative velocity, W_1, is highest, the calculation is based only on the maximum diameter of the blade tip at impeller entry. Due to the non-complex geometry of the test rig suction intake, a K_1 value of 1.2 was used. The incidence angle alpha that influences K_2 is the difference between the inlet blade angle and flow angle. A suggested minimum value of K_2 for conventional pumps with a good impeller inlet design is 0.25, as can be seen in Figure 22 [9]. However, because of the detailed analysis techniques used to minimize flow acceleration at the blade leading edge of the impeller, a K_2 value of 0.18 was estimated.

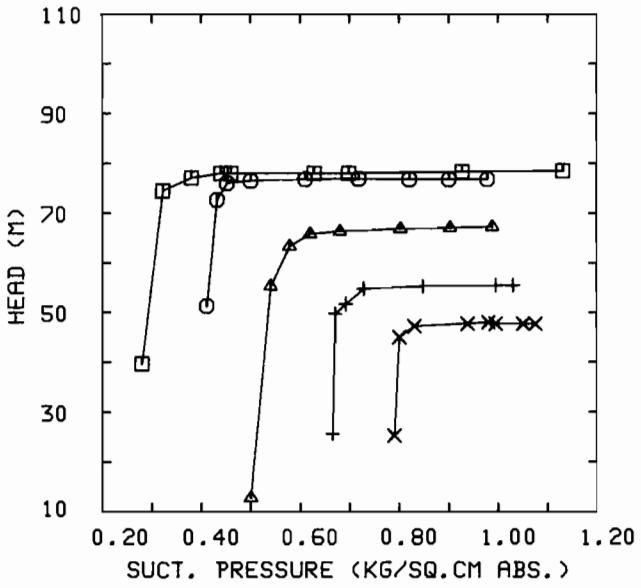

(□)... 50 CU.M/H (○)... 75 CU.M/H
(△)... 105 CU.M/H (+)... 130 CU.M/H
(×)... 145 CU.M/H

Figure 20. Head Drops Measured in Low-Speed Cavitation Tests.

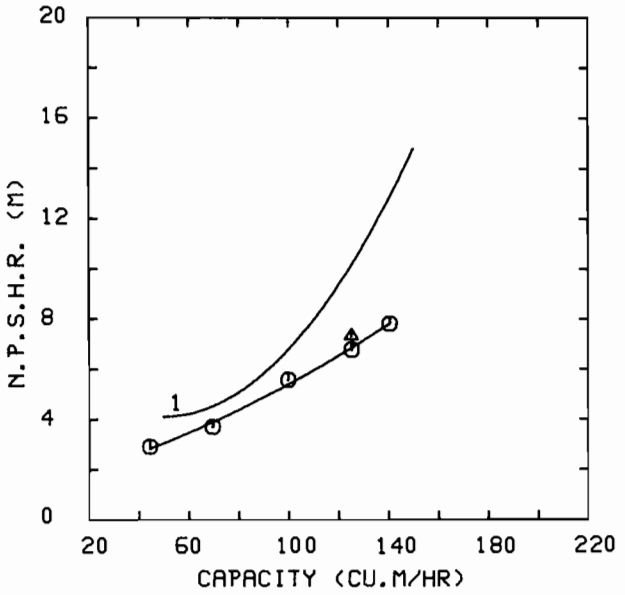

1..... PREDICTED (○)... TEST 3% LOSS
(△)... CAV. FREE

Figure 21. Predicted and Experimental $NPSH_R$ at Low Speed.

This low value appears reasonable when substantiated by the blade-pressure distribution provided in the computer blade-to-blade flow analysis output.

Lastly, head-capacity and constant hydraulic efficiency lines for three different outside-impeller-diameter trims are shown in Figure 23. The maximum efficiency area is centered around the five percent diameter cut, as a result of the reduction in the impeller disk friction. This could also have been anticipated

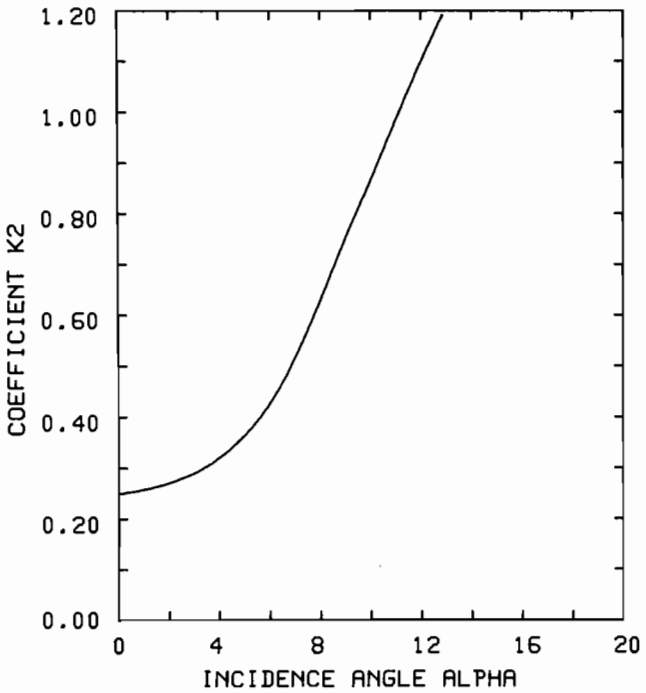

Figure 22. K_2 Coefficients for $NPSH_R$ Evaluations [9].

from the initial parametric study, indicating some efficiency benefits with many stages having small diameter impellers (Figure 7). The small changes in the maximum stage efficiency for all trims makes it possible to cover the ranges of applications of the Figure 6 performance chart with little or no change in speed. This feature allows the best efficiency speed for the gas turbine to be maintained in the majority of matching with pumps of this family.

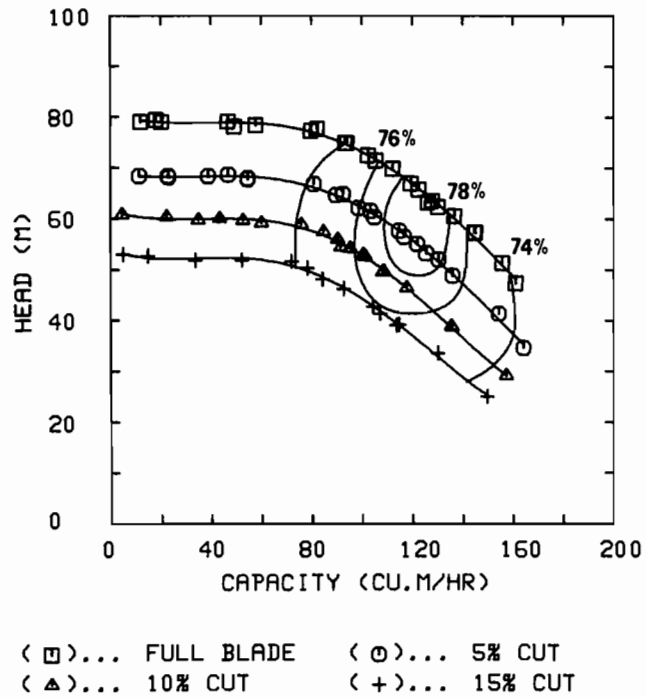

Figure 23. Low-Speed Performance for Different Impeller Trims.

Balance-Drum Seal Tests

The in-line stage arrangement needs good sealing across the balancing drum, to achieve high volumetric efficiencies. An experimental program was carried out to check different seal geometries. The study was made on a device provided with a drum rotating at full pump speed. The tests included the measurement of the α coefficient, used in Blasius' expression of the equivalent seal friction factor [10, Chapter 1]:

$$\lambda = \frac{\alpha}{(Re)^{0.25}}$$

The experimental α coefficients are shown in Figure 24; all are referred to 0.056, the straight seal value [10], checked and validated during this testing. Several spiral groove seals, with different shapes of cavities, gave results far better than other geometries. The particular seal geometry utilized on the high speed pump unit tested was a version of the best performing spiral seal, slightly modified for manufacturing constraints. It provided an α coefficient 6.5 times higher than that of the plain seal.

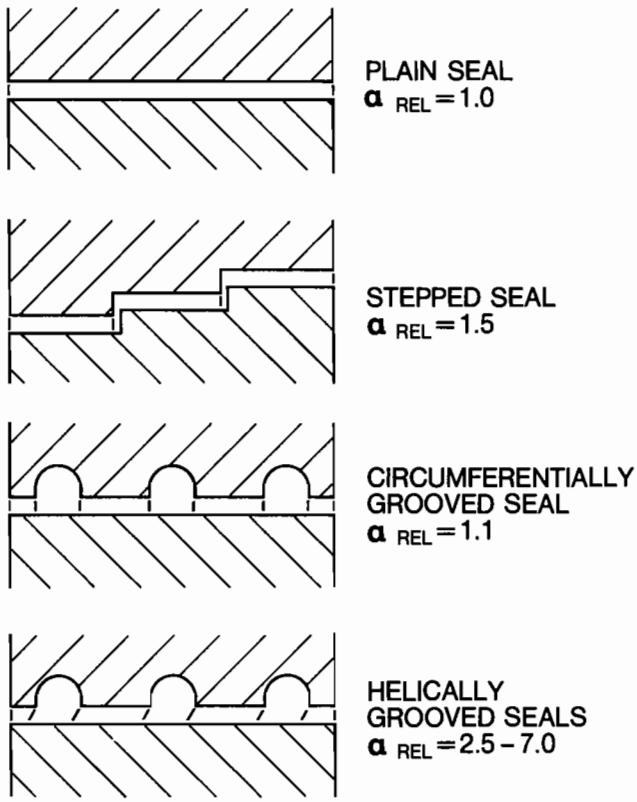

Figure 24. Results of Balancing Drum Seal Leakage Tests.

Evaluation of the Radial Bearing Characteristics

The radial bearings used on this pump are standard, five-tilting-pad type currently utilized on high-speed centrifugal compressors and gas turbines. No special work was necessary to evaluate their stiffness and damping oil-film coefficients for use in the rotordynamic analysis. In fact, they had already been extensively studied on a special in-house facility (Figure 25) available for development of high speed journal bearings. It consists of a bearing housing hydraulically vibrated over a rigidly supported rotating shaft. By correlating applied forces to

housing displacements via a computerized mathematical procedure, the 4 + 4 oil-film stiffness and damping coefficients can be evaluated. As an example, in Figure 26, the experimental stiffness coefficients of a standard five-pad bearing are compared with predictions made with a finite-element, lubrication-theory analysis.

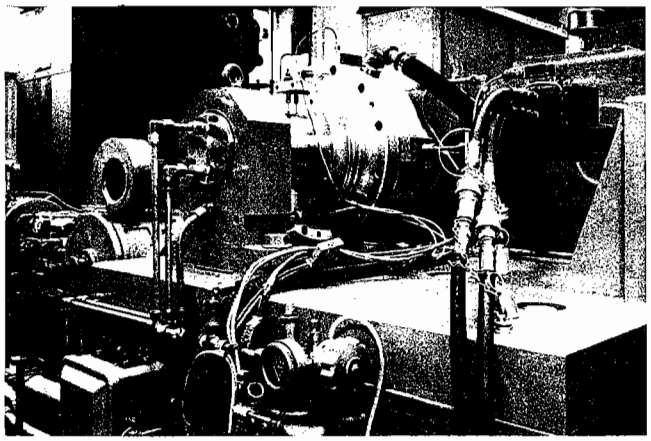

Figure 25. Facility for Evaluation of Journal Bearing Oil-Film Rotordynamic Coefficients.

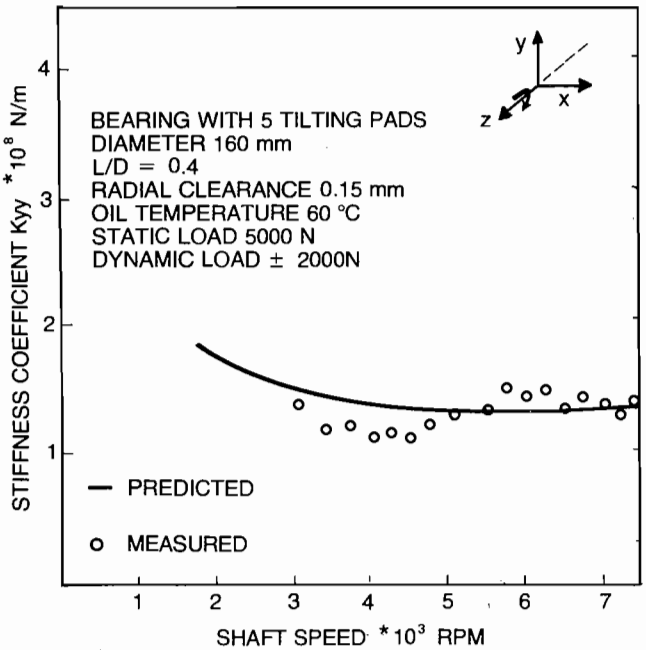

Figure 26. Standard Tilting-Pad Bearing Predicted and Experimental Stiffness Coefficients.

FULL-LOAD TESTS OF A GAS-TURBINE-DRIVEN HIGH-SPEED PUMP UNIT

The first high-speed pump unit driven by its matching gas turbine was run on the shop faciity available for full-power testing of complete turbounits [11]. The test setup (Figure 27) was fully representative of a complete turbopump module. The pump was fully integrated with the turbine's auxiliaries and control system, with the two individual skids bolted together to form a single structure.

To check the pump's overall efficiency, shaft torque was measured by means of a high-speed calibrated torquemeter. To

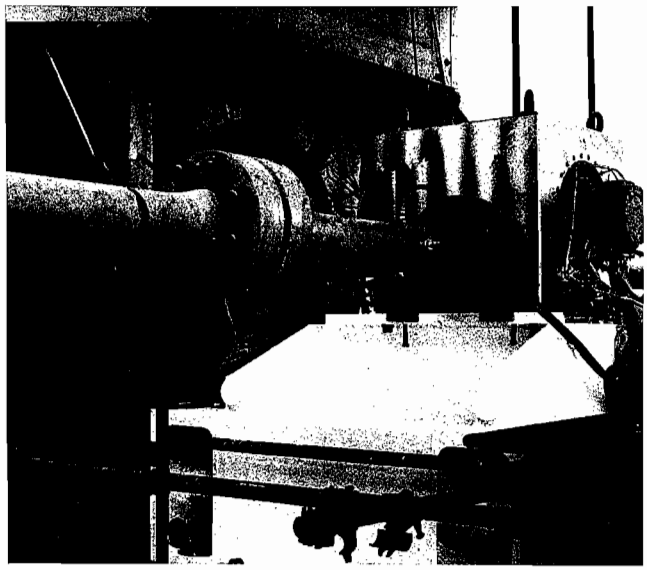

Figure 27. Test Setup of a High-Speed Pump and Two-Shaft Gas Turbine Integrated Assembly.

check the power measurement through the pump thermal balance, calibrated thermocouples were used to measure the water-temperature rise (around 9°C or 48°F at full power) between suction and discharge. Estimated power measurement precision at full power with torquemeter and water thermal balance were ±1.5 percent and ±3.5 percent, respectively. This estimate was based on the standard deviation curves of the instruments with a confidence interval of $\pm 2\sigma$. Most power measurements, made through both types of readings, were within a scatter band within one percent of the maximum 6,000 hp power. Torquemeter predictions of power were slightly higher than values resulting from the energy balance; a similar trend for these kinds of measurements has also resulted in previous load tests of different types of machines [12]. Six Kiel probe rakes for total pressure measurements were installed upstream of the first impeller intake. They were used to check the possible pressure distortions coming from the intake which were not present on the low speed stage rig.

Shaft vibrations measured with eddy-current probes were continously monitored and analyzed by a FFT unit, and recorded for subsequent investigations. All readings and real-time data reduction were performed by a central data acquisition system serving the shop test facilities.

A summary of the pump's hydraulic performance can be seen in Figure 28. The predicted heads and efficiencies also shown were evaluated from the experimental low-speed stage hydraulic performance. For this purpose, estimated pump intake and discharge losses and balancing drum seal leakage losses were added to low-speed performance, and no Reynolds number corrections were applied. Measured head-capacity points appear to be slightly below the curve predicted from single-stage tests, with no inlet swirl. This is likely due to the mutual interference among the stages operating in series, with some residual swirl left at the exit of the return channels. This fact is commonly observed on multistage centrifugal compressors, consisting of stacks of stages each tested individually [13, 14].

The overall test efficiencies, evaluated with the torquemeter power measurements, appear to be consistent with predictions based on the low-speed tests, and confirm the interpretation of the observed shifts in the pump's measured head-capacity curve. The rotordynamic behavior was quite satisfactory over the full speed range, as can be observed from the time histories

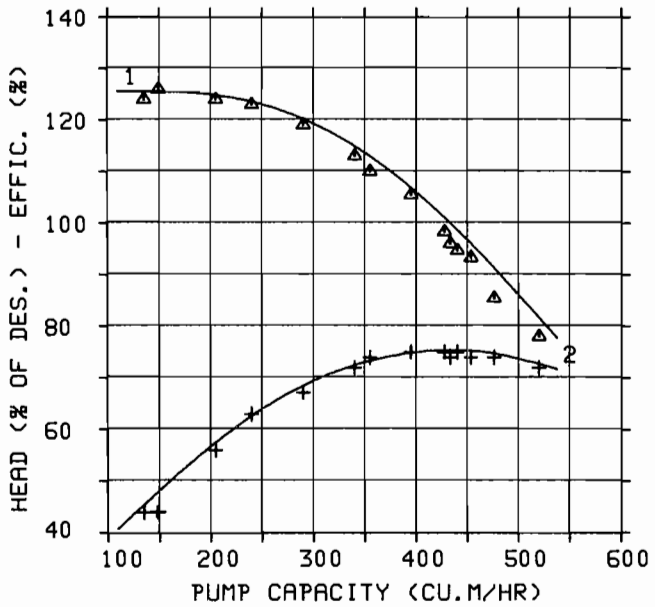

1..... PRED.HEAD 2..... PRED.EFFIC.
(▲)... TEST HEAD (+)... TEST EFFIC.

Figure 28. High-Speed Pump Predicted and Tested Performance at 10290 CPM.

of the shaft vibrations at the two bearings shown in Figure 29, for acceleration through the complete speed range. No significant vibration amplifications appear; this confirms the predicted absence of rotor critical speeds for a wet-running pump over the entire speed range.

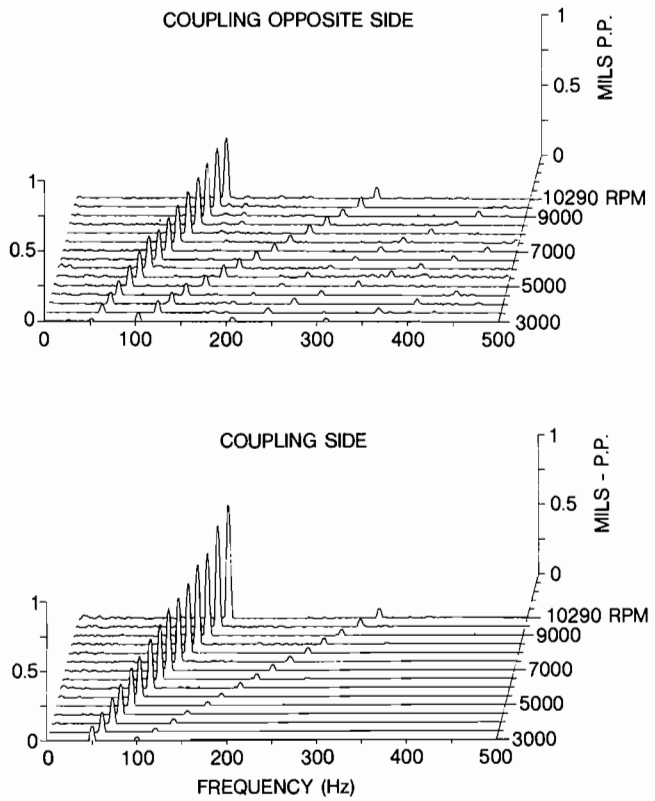

Figure 29. Time-Histories of Shaft Vibrations at the Bearings.

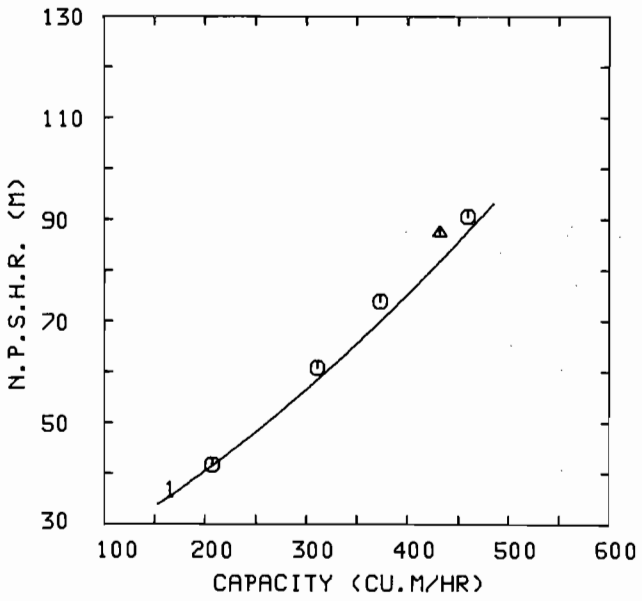

1..... PRED.3% LOSS (⊙)... TEST 3% LOSS
(▲)... CAV. FREE

Figure 30. Predicted and Measured Pump $NPSH_R$ at 10290 CPM.

$NPSH_R$ values demonstrated during full load testing at 10,290 cpm compare favorably with cavitation-free $NPSH_R$ and the 2,980 cpm $NPSH_R$ values taken up by the square law. Results shown in Figure 30 suggest a K_1 value of 1.3 for cavitation free $NPSH_R$ and confirm appropriate intake design with minimum friction and acceleration losses. The total pressure measurements made upstream of the first impeller inlet validate these results. In fact, no meaningful average total pressure drop from the suction nozzle could be recorded with these instruments, while the peak-to-peak total pressure distortion did not exceed three percent of the mean value. Therefore, the first-stage inlet flow conditions achieved on the complete pump can be considered equivalent to those present on the low-speed stage facility with axial intake to the impeller.

CONCLUSIONS

The development of a compact, high-speed centrifugal pump with good efficiency, favorable suction characteristics, and stable rotordynamic behavior has been successfully demonstrated. The design is optimized for using a two-shaft gas turbine as first choice driver. This allows the users to change the pump output in a wide range through speed control preserving efficiency. This feature can be very helpful in injection services to offset uppredictable changes in well requirements during exploitation. The direct coupling without gear of the pump with heavy-duty gas turbine models results in a compct and simple assembly which is easy to transport and install. Other advantages are small foundation size, easy alignment and reduced maintenance. Additional features that favor users' on-site maintenance have been successfully demonstrated and widely used on high-pressure centrifugal compressors. These include the horizontally-split diffuser diaphragms and a split inner casing forming a single and easily replaceable cartridge. Lastly, the limited cavitation-free $NPSH_R$ levels which have been demonstrated help to keep inlet boosting powers within the limits of low-voltage electric motor capabilities. This feature is favorable, especially for off-shore applications.

In summary, besides providing users with the performance and reliabilitiy requisities they normally expect, the high speed pump which has been developed has features that should favor its applications in the oil industry in general, and in high-pressure-injection service in particular.

REFERENCES

1. Benvenuti, E., "Aerodynamic Development of Stages for Industrial Centrifugal Compressors. Part 1: Testing Requirements and Equipment—Immediate Experimental Evidence," ASME Paper No. 78-GT-4 (1978).
2. Benvenuti, E., "Aerodynamic Development of Stages for Industrial Centrifugal Compressors. Part 2: Test Data Analysis, Correlation and Use," ASME Paper No. 78-GT-5 (1978).
3. Benvenuti, E. and Lacitignola, P., "Analytical and Experimental Procedures for Rotordynamics Predictions During Development of New Turbomachines," Proceedings of International IFTOMM Conference, Rotordynamic Problems in Power Plants, Rome, Italy, pp. 469-495 (1982).
4. Fraser, W.H., "Flow Recirculation in Centrifugal Pumps," Proceedings of the Tenth Turbomachinery Symposium, Turbomachinery Laboratories, Department of Mechanical Engineering, Texas A&M University, College Station, Texas, pp. 95-100 (1981).
5. Fraser, W.H., "Avoiding Recirculation in Centrifugal Pumps," Machine Design, pp. 87-91 (June 10, 1982).
6. Brophy, M.C., "Computer Assisted Design of Pump Impellers," Technical Memorandum TM 78-02, Applied Research Laboratory, Pennsylvania State University (January 1978).
7. Perferi, A., "Calculation of Flexural Vibration Amplitude and of Damped Natural Frequencies of Flexural Vibrations," Nuovo Pignone Internal Report (September 1978).
8. Lomakin, A.A., "Calculation of Critical Speed and Securing of Dynamic Stability of Hydraulic High Pressure Pumps with Reference to Forces Arising in Seal Gaps," Energomachinostroenie 4(1), p. 1158 (1958).
9. Lobanoff, V.S. and Ross, R.R., *Centrifugal Pumps—Design & Application*, Houston, Texas: Gulf Publishing Company (1985).
10. Lazarkiewicz, S., and Troskolanski, A.T., *Impeller Pumps*, First Edition, Warsaw, Poland: Pergamon Press (1965).
11. Giovannini, M., Maretti, A. and Nava, P.L., "Shop Full-Load Testing of Centrifugal Compressors," *Proceedings of the Eleventh Turbomachinery Symposium*, Turbomachinery Laboratories, Department of Mechanical Engineering, Texas A&M University, College Station, Texas, pp. 113-120 (1982).
12. Lacitignola, P., and Valentini, E., "Development of the PGT 25 High Efficiency Gas Turbine. Part 3: Experimental Program and Testing," ASME Paper No. 84-GT-63 (1984).
13. Benvenuti, E., "Development Testing of Stages for Process Centrifugal Compressors," Paper presented "Industrial Centrifugal Compressors," lecture series, Von Karman Institute for Fluid Dynamics, Brussels, Belgium (February 1977).
14. Benvenuti, E., Bonciani, L. and Corradini, U., "Inlet Flow Distorsions on Centrifugal Compressor Stages—Experimental Investigations and Evaluation of Effects on Performance," AGARD-CP-282 (November 1980).